Mathematical Geology, Vol. 36, No. 8, November 2004 (© 2004)

The Bingham Distribution of Quaternions and Its Spherical Radon Transform in Texture Analysis[1]

Karsten Kunze[2] and Helmut Schaeben[3]

Spherical geometry of quaternions is employed to characterize the Bingham distribution on the 3-dimensional sphere $\mathbb{S}^3 \subset \mathbb{R}^4$ as being uniquely composed of a bipolar, a circular and a spherical component. A new parametrization of its dispersion parameters provides a classification of patterns of crystallographic preferred orientations (CPO, or textures). It is shown that the Bingham distribution can represent most types of ideal CPO patterns; in particular single component, fiber and surface textures are represented by rotationally invariant bipolar, circular and spherical distributions, respectively. Pole figures of given crystal directions are derived by the spherical Radon transform of the Bingham probability density function of rotations, which are displayed for general and special cases.

KEY WORDS: rotations, crystallographic preferred orientations, texture components, fiber textures, pole figures, spherical statistics.

INTRODUCTION

Crystallographic preferred orientations (CPO) of minerals in rocks are commonly used to infer constraints on their tectono-metamorphic history (e.g., Wenk, 1985). They are usually presented and discussed as pole figures (fabric diagrams) of some specific crystal planes or directions. The actual frequency distribution of crystal orientations typically receives less attention, even though it provides the basic link between the diverse pole figures, because it is harder to visualize in an intuitive fashion.

Model orientation distributions aid in interpreting CPO patterns, as they are characterized by a rather small number of meaningful parameters, which may be the centers of concentration or depletion, the degree and anisotropy of scattering, or certain patterns of rotational symmetry and invariance. They provide hypotheses

[1]Received 17 December 2003; accepted 27 July 2004.

[2]Department of Earth Sciences, ETH Zurich, CH-8092 Zurich, Switzerland; e-mail: karsten.kunze@erdw.ethz.ch

[3]Geoscience Mathematics and Informatics, University of Mining and Technology, D-09596 Freiberg, Germany; e-mail: schaeben@geo.tu-freiberg.de

0882-8121/04/1100-0917/1 © 2004 International Association for Mathematical Geology

for measured data to be tested against by statistical methods. The Bingham distribution is well suited for this purpose, as its parameter domain allows to simulate a wide range of different CPO; preliminary results were given by Schaeben (1996).

Neglecting crystal symmetry for the sake of simplicity, a crystallographic orientation is a rotation between the individual crystal and the specimen. The frequency of crystal orientations in a representative polycrystalline sample volume is given by the orientation (probability) density function (ODF) $f\colon SO(3) \mapsto \mathbb{R}^1_+$. If rotations are represented by unit quaternions, the ODF is an even function defined on $\mathbb{S}^3 \subset \mathbb{R}^4$. Pole figures are derived by the spherical Radon transform $\mathcal{R}f$ of the ODF f, representing the probability distribution of a given unit vector $\mathbf{h} \in \mathbb{S}^2 \subset \mathbb{R}^3$, i.e., of a specific direction in a crystal, which has been subjected to a random rotation with a given—say Bingham—distribution f.

In this contribution we will show that the Bingham distribution of unit quaternions is uniquely composed of distinct amounts to a bipolar, a circular and a spherical component, which is made transparent by a new parametrization of the dispersion parameters. We will particularly discuss the limiting cases, for which the Bingham distribution degenerates to rotationally invariant distributions, and which are related to known basic CPO types such as single orientation components, fiber textures and surface textures. It is further demonstrated, how transitional cases of the Bingham distribution relate to intermittent texture types. Pole figures for general and special cases are derived by the spherical Radon transform. It is shown by example that very different, even complementary, orientation distributions may give rise to hardly distinguishable pole figures, at least for certain crystal directions, stressing the point to rely on the entire orientation distribution when characterizing the CPO of a rock.

ROTATIONS AND QUATERNIONS

The orientation $\boldsymbol{g}$ of an individual crystal in a polycrystalline sample is the active rotation $\boldsymbol{g} \in SO(3) : K_S \mapsto K_C$ that maps a right-handed orthonormal coordinate system K_S fixed to the specimen onto another right-handed orthonormal coordinate system K_C fixed to the crystal,

$$\boldsymbol{g}K_S = K_C, \quad \boldsymbol{g} \in SO(3). \tag{1}$$

If a unique direction is represented by unit vector $\mathbf{h}$ with respect to the crystal frame K_C, and by unit vector $\mathbf{r}$ with respect to the specimen frame K_S, then the coordinates of the unique direction transform according to

$$\mathbf{r}_{K_S} = \boldsymbol{g}\mathbf{h}_{K_C}. \tag{2}$$

The rotation $\boldsymbol{g}$ may be represented by a (3×3) orthogonal matrix $X(\boldsymbol{g})$ such that

$$\mathbf{r} = X(\boldsymbol{g})\mathbf{h},$$

where matrix multiplication applies, or by a unit quaternion $q(\boldsymbol{g}) \in \mathbb{S}^3$ such that

$$\mathbf{r} = q(\boldsymbol{g})\mathbf{h}\, q^*(\boldsymbol{g}) \tag{3}$$

where quaternion multiplication applies.

The quaternion representation will be pursued here as it proved particularly appropriate to treat statistics of rotations by spherical statistics. Basic properties of quaternions are compiled in the Appendix.

Quaternion Representation of Rotations in $\mathbb{R}^3$

Equations (2) and (3) explicitly read (e.g., Altmann, 1986)

$$\mathbf{r} = \boldsymbol{g}\,\mathbf{h} = q\,\mathbf{h}\,q^* = \mathbf{h}\,\cos\omega + (\mathbf{n} \times \mathbf{h})\,\sin\omega + (\mathbf{n} \cdot \mathbf{h})\,\mathbf{n}(1 - \cos\omega)$$

using the parametrization of unit quaternions by rotation axis $\mathbf{n}$ and rotation angle ω [Appendix, Eq. (33)].

Both unit quaternions $\pm q \in \mathbb{S}^3$ represent one and the same rotation in $\mathbb{R}^3$, i.e., $\mathbb{S}^3$ stands for a double covering of the group $SO(3)$. The unit sphere $\mathbb{S}^2 \subset \mathrm{Vec}\mathbb{H}$ consists of all quaternions representing rotations by the angle π about arbitrary axes in $\mathbb{S}^2$, as every unit vector $\mathbf{q}$ can be considered as the pure quaternion $q = \cos(\pi/2) + \mathbf{q}\,\sin(\pi/2)$. The unit quaternions $\pm q^*$ represent the inverse rotation $\boldsymbol{g}^{-1}\mathbf{r} = \mathbf{h}$ by angle ω and axis $-\mathbf{n}$.

Henceforward, no distinction will be made between the rotation $\boldsymbol{g}$ and its (up to the sign) unique quaternion representation q. Similarly, a unit vector $\mathbf{q} \in \mathbb{S}^2 \subset \mathrm{Vec}\mathbb{H}$ is identified with its corresponding pure unit quaternion $q = (0 + \mathbf{q}) \in \mathbb{S}^3 \subset \mathbb{H}$, for which the rules of quaternion multiplication apply. Both will be denoted here by $\mathbf{q}$; the distinction is made by context.

In terms of passive rotations, Equation (2) provides the coordinate transformation of a unique vector given by $\mathbf{h}_{K_\mathcal{C}}$ or $\mathbf{r}_{K_\mathcal{S}}$ with respect to the crystal $(K_\mathcal{C})$ or the specimen $(K_\mathcal{S})$ coordinate system, respectively, that are related to each other by the rotation $\boldsymbol{g}$: $K_\mathcal{S} \mapsto K_\mathcal{C}$. The commonly applied convention in texture analysis (Bunge, 1982) is — in a strict mathematical sense incorrectly — to use one and the same unique symbol g to refer to both the (active) rotation $\boldsymbol{g}$ of coordinate systems $\boldsymbol{g}\,K_\mathcal{S} = K_\mathcal{C}$ and the (passive) transformation $\boldsymbol{g}^{-1}$ of unit vectors $\mathbf{h}_{K_\mathcal{C}} = \boldsymbol{g}^{-1}\,\mathbf{r}_{K_\mathcal{S}}$. Formal consistency based on the vector transformation rule [Eq. (2)] is maintained

between previous references and the formulae given here by identifying $\boldsymbol{g} = g^{-1}$, and vice versa.

Additional details concerning the geometry of rotations when represented by unit quaternions are given by Meister and Schaeben (2004).

Parameterizations of Unit Quaternions

Any set of four orthonormal quaternions $a_i \in \mathbb{S}^3, i = 1, \ldots, 4$, spans the sphere $\mathbb{S}^3$ of all unit quaternions, which may be parameterized in either way by

$$q(r,s,t) = ((a_1 \cos t + a_2 \sin t) \sin s + a_3 \cos s) \sin r + a_4 \cos r, \quad \text{or} \tag{4}$$

$$q(r,s,t) = (a_1 \cos t + a_2 \sin t) \sin s + (a_3 \sin r + a_4 \cos r) \cos s. \tag{5}$$

$$\mathbb{S}^3 = \{q(r,s,t) \in \mathbb{H} \,|\, r, s \in [0,\pi], \quad t \in [0, 2\pi)\}$$

If the quaternions a_i are identified with the basis in $\mathbb{H}$ by $a_i = e_i, i = 1, \ldots, 3$, and $a_4 = 1$, then the variables are easily interpreted. Since any rotation is represented twice in $\mathbb{S}^3$ (by q and $-q$), the parameter domains for the following rotations cover half of $\mathbb{S}^3$.

- In the first case [Eq. (4)] they correspond to rotation angle $\omega \in [0, \pi]$ and axis $\mathbf{n} \in \mathbb{S}^2$ as introduced by Equation (33) according to

$$r = \omega/2, \quad s = \theta, \quad t = \varphi, \tag{6}$$

  where $\theta \in [0, \pi]$ and $\varphi \in [0, 2\pi)$ are the spherical angles of the rotation axis $\mathbf{n} = (\cos\varphi \sin\theta,\ \sin\varphi \sin\theta,\ \cos\theta)^t$.
- In the second case [Eq. (5)] they correspond to linear combinations of the Euler angles (ϕ_1, Φ, ϕ_2) conventionally used in texture analysis (Bunge, 1982) with $(\phi_1,\ \phi_2 \in [0, 2\pi); \Phi \in [0, \pi])$

$$r = (\phi_1 + \phi_2)/2, \quad s = \Phi/2, \quad t = (\phi_1 - \phi_2)/2. \tag{7}$$

- The variables in Equation (5) may alternatively be interpreted in terms of a product pq of two rotations represented by $p, q \in \mathbb{S}^3$ about mutually perpendicular axes. Let p and q have rotation axes parallel and perpendicular to e_3, respectively, i.e.,

$$p = \cos\frac{\omega_p}{2} + \sin\frac{\omega_p}{2} e_3,$$

$$q = \cos\frac{\omega_q}{2} + \sin\frac{\omega_q}{2}(\cos\varphi_q e_1 + \sin\varphi_q e_2),$$

with $\omega_p,\ \varphi_q \in [0, 2\pi); \omega_q \in [0, \pi]$. Then the parameters are given by

$$r = \omega_p/2, \quad s = \omega_q/2, \quad t = \omega_p/2 + \varphi_q.$$

Points, Circles and Spheres in $\mathbb{S}^3$

Let $a_i \in \mathbb{S}^3, i = 1, \ldots, 4$, be any set of four orthonormal quaternions. Let $L(a_4) \subset \mathbb{H}$ be a line parallel to a_4, $E(a_3, a_4) \subset \mathbb{H}$ be a plane spanned by a_3, a_4, and $F(a_2, a_3, a_4) \subset \mathbb{H}$ be a hyperplane spanned by a_2, a_3, a_4. Their intersections with $\mathbb{S}^3$ constitute a single bipolar unit quaternion $B(a_4)$, a unit circle $C(a_3, a_4)$, or a unit sphere $S(a_2, a_3, a_4)$, which are of dimension zero, one or two, respectively, and given by

$$\begin{aligned}
B(a_4) &:= L(a_4) \cap \mathbb{S}^3 = \{-a_4, +a_4\},\\
C(a_3, a_4) &:= E(a_3, a_4) \cap \mathbb{S}^3\\
&= \{q(t) \in \mathbb{S}^3 \mid q(t) = a_4 \cos t + a_3 \sin t, t \in [0, 2\pi)\},\\
S(a_2, a_3, a_4) &:= F(a_2, a_3, a_4) \cap \mathbb{S}^3\\
&= \{q(s, t) \in \mathbb{S}^3 \mid q(s, t) = (a_4 \cos t + a_3 \sin t) \sin s + a_2 \cos s,\\
&\quad \times s \in [0, \pi],\ t \in [0, 2\pi)\}.
\end{aligned} \tag{8}$$

Obviously, $B(a_1)$ and $S(a_2, a_3, a_4) =: a_1^{\perp}$ are mutually orthogonal complements with respect to $\mathbb{S}^3$, and so are $C(a_3, a_4)$ and $C(a_1, a_2)$. These circles and spheres are centered at $\mathcal{O}$, the origin of the coordinate system; thus they are geodetic lines or surfaces, respectively.

The orientation distances between $x \in \mathbb{S}^3$ and a bimodal point, a circle or a sphere are derived from orthogonal projections of x onto L, E, or F, respectively, as

$$\begin{aligned}
\cos^2 \frac{\omega_b}{2} &= (\mathrm{Sc}(a_4^* x))^2 = 1 - (\mathrm{Sc}(a_3^* x))^2 - (\mathrm{Sc}(a_2^* x))^2 - (\mathrm{Sc}(a_1^* x))^2,\\
\cos^2 \frac{\omega_c}{2} &= (\mathrm{Sc}(a_4^* x))^2 + (\mathrm{Sc}(a_3^* x))^2 = 1 - (\mathrm{Sc}(a_2^* x))^2 - (\mathrm{Sc}(a_1^* x))^2,\\
\cos^2 \frac{\omega_s}{2} &= (\mathrm{Sc}(a_4^* x))^2 + (\mathrm{Sc}(a_3^* x))^2 + (\mathrm{Sc}(a_2^* x))^2 = 1 - (\mathrm{Sc}(a_1^* x))^2,
\end{aligned} \tag{9}$$

where ω_b denotes the orientation distance between x and the bimodal point $B(a_4)$, ω_c the one between x and the circle $C(a_3, a_4)$, and ω_s the one between x and the sphere $S(a_2, a_3, a_4)$.

For vectors $\mathbf{h}_c, \mathbf{r}_c \in \mathbb{S}^2$ defined by

$$\begin{aligned}
\mathbf{h}_c &:= \mathrm{Vec}(a_4^* a_3) = a_4^* a_3 = -a_3^* a_4 = \mathrm{Vec}(a_2^* a_1) = a_2^* a_1 = -a_1^* a_2,\\
\mathbf{r}_c &:= \mathrm{Vec}(a_3 a_4^*) = a_3 a_4^* = -a_4 a_3^* = -\mathrm{Vec}(a_1 a_2^*) = -a_1 a_2^* = a_2 a_1^*,
\end{aligned} \tag{10}$$

the circle $C(a_3, a_4)$ represents the set of all rotations mapping $\mathbf{h}_c$ on $\mathbf{r}_c$, i.e., $q\,\mathbf{h}_c\,q^* = \mathbf{r}_c$ for all $q \in C(a_3, a_4)$. The complementary circle $C(a_1, a_2)$ is the set of all rotations mapping $\mathbf{h}_c$ on $-\mathbf{r}_c$ (Kunze, 1991; Meister and Schaeben, 2004). The orientation distance ω_c is also given by $\cos\omega_c = \mathbf{r}_c \cdot x\,\mathbf{h}_c\,x^*$ as follows using the decomposition $x = \sum_{i=1}^{4} x^i a_i$ with $x^i = \mathrm{Sc}(a_i^* x)$

$$\begin{aligned}\mathbf{r}_c \cdot x\mathbf{h}_c\,x^* &= -\,\mathrm{Sc}(\mathbf{r}_c\,x\,\mathbf{h}_c\,x^*) = -\,\mathrm{Sc}(a_3 a_4^* x\,a_4^* a_3\,x^*)\\ &= -\sum_{i=1}^{4}\sum_{j=1}^{4} x^i x^j\,\mathrm{Sc}(a_3 a_4^* a_i\,a_4^* a_3\,a_j^*) = -(x^1)^2 - (x^2)^2 + (x^3)^2 + (x^4)^2\\ &= 2\,[(\mathrm{Sc}(a_3^* x))^2 + (\mathrm{Sc}(a_4^* x))^2] - 1 = 2\cos^2\frac{\omega_c}{2} - 1 = \cos\omega_c.\end{aligned}$$

For any pair $\mathbf{h}, \mathbf{r} \in \mathbb{S}^2$ with $a_1 \mathbf{h} a_1^* = \mathbf{r}$, the sphere $S(a_2, a_3, a_4) = a_1^{\perp} = \mathbb{S}^2 a_1 \subset \mathbb{S}^3 \subset \mathbb{H}$ contains the circle representing all rotations mapping $\mathbf{h}$ on $-\mathbf{r}$, and it does not contain any other circle mapping $\mathbf{h}$ on a direction different of $-\mathbf{r}$ (Meister and Schaeben, 2004).

Invariant Measures in $\mathbb{S}^3$

Let $\mathbb{S}^3$ be embedded in $\mathbb{R}^4$ so that $p = cq \in \mathbb{R}^4$, $q \in \mathbb{S}^3$, $c \in \mathbb{R}$. Then the invariant measure on $\mathbb{S}^3$ is obtained from the (unsigned) Jacobian for the transformation from (p_0, p_1, p_2, p_3) to (c, r, s, t) for $c = 1$, which reads from Equations (4) and (6)

$$ds_3 = \sin^2 r\,\sin s\,dr\,ds\,dt = \frac{1}{2}\,\sin^2\frac{\omega}{2}\,\sin\theta\,d\omega\,d\theta\,d\varphi,$$

or from Equations (5) and (7) it is

$$ds_3 = \sin s\,|\cos s|\,dr\,ds\,dt = \frac{1}{8}\,\sin\Phi\,d\Phi\,d\phi_1\,d\phi_2. \tag{11}$$

Notice that ds_3 is $1/8$ of $dg = \sin\Phi\,d\Phi\,d\phi_1\,d\phi_2 = 4\,\sin^2\frac{\omega}{2}\,\sin\theta\,d\omega\,d\theta\,d\varphi$, which is commonly defined in texture analysis yielding $\int_{SO(3)} dg = 8\pi^2$. Further recall that $SO(3)$ is covered twice by $\mathbb{S}^3$.

From Equations (4) and (6), the invariant measure on the sphere is analogously obtained for $c = 1$, $\omega = 2r = \pi$

$$ds_2 = \sin s\,ds\,dt = \sin\theta\,d\theta\,d\varphi, \tag{12}$$

and the invariant measure on the circle is found for $c = 1$, $\omega = 2r = \pi$, $\theta = s = \pi/2$ as

$$ds_1 = dt = d\varphi.$$

Integration results in

$$\int_{\mathbb{S}^3} ds_3 = \int_0^{\pi} \sin^2 r \, dr \int_{\mathbb{S}^2} ds_2 = 2\pi^2, \tag{13}$$

$$\int_{\mathbb{S}^2} ds_2 = \int_0^{\pi} \sin s \, ds \int_{\mathbb{S}^1} ds_1 = 4\pi, \tag{14}$$

$$\int_{\mathbb{S}^1} ds_1 = \int_0^{2\pi} dt = 2\pi.$$

THE BINGHAM DISTRIBUTION ON $\mathbb{S}^3$

General Definition

Let $x \in \mathbb{S}^3 \subset \mathbb{H}$ be a unit quaternion representing a random rotation. Then x is said to be distributed according to the (even) Bingham distribution $B_4(\Lambda, A)$ (Bingham, 1964, 1974) if it has the probability density function

$$f_{\mathrm{B}}(x; \Lambda, A) = c_B^{-1}(\Lambda) \exp\left\{ \sum_{i=1}^{4} \lambda_i (\mathrm{Sc}(a_i^* x))^2 \right\} [ds_3], \tag{15}$$

where ds_3 represents the Lebesgue invariant measure on $\mathbb{S}^3$, $A \in SO(4)$ is a (4×4) orthogonal matrix with unit column quaternions $a_i \in \mathbb{S}^3 \subset \mathbb{H}$ such that $\sum_{i=1}^{4} (\mathrm{Sc}(a_i^* x))^2 = 1$, Λ is a (4×4) diagonal matrix with entries $\lambda_1, \ldots, \lambda_4$, and $c_B(\Lambda)$ is a normalizing constant. It should be noted that $B_4(\Lambda + \alpha I_4, A)$ and $B_4(\Lambda, A)$ are indistinguishable for any $\alpha \in \mathbb{R}$, i.e., the shape parameters λ_i, $i = 1, \ldots, 4$, are only determined up to an additive constant. Uniqueness can be imposed by some convention as suggested in the following section.

Since the numbers $\mathrm{Sc}(a_i^* x)$ correspond to the usual inner product $a_i \cdot x$ of a_i and x taken as elements of $\mathbb{R}^4$, they may be geometrically interpreted as the direction cosines of a random quaternion x with respect to the mutually orthogonal "modes" a_i.

Following Prentice (1986), different sets of (sorted) entries of Λ in Equation (15) give

- a bimodal "bipolar" distribution, if $\lambda_1 + \lambda_4 > \lambda_2 + \lambda_3$,
- a multimodal "circular" distribution, if $\lambda_1 + \lambda_4 = \lambda_2 + \lambda_3$,
- a multimodal "spherical" distribution, if $\lambda_1 + \lambda_4 < \lambda_2 + \lambda_3$,
- the uniform distribution if $\lambda_1 = \lambda_2 = \lambda_3 = \lambda_4$.

The respective sets of modes of dimension 0, 1, 2, or 3 are constituted by the a_i corresponding to the (positive) greatest of the λ_i.

What we have just termed "spherical" here refers to the label "equatorial girdle" by Prentice (1986), who considered any 2-dimensional subsphere with the origin $\mathcal{O}$ as center and spanned by three mutually orthogonal vectors of $\mathbb{S}^3 \subset \mathbb{H}$ as a great–circle in $\mathbb{S}^3$. Since 1-dimensional subspheres, i.e., circles with center $\mathcal{O}$ spanned by two quaternions in $\mathbb{S}^3 \subset \mathbb{H}$, play a prominent role in texture analysis, the term equatorial girdle is avoided here as it does not properly indicate the geometry and dimension of the set of modes.

Bipolar, Circular and Spherical Distributions

Prentice (1986) labeled the λ_i such that $\lambda_1 \le \lambda_2 \le \lambda_3 \le \lambda_4$ in the bipolar case, but $\lambda_1 \ge \lambda_2 \ge \lambda_3 \ge \lambda_4$ in the spherical case. Since this labeling seems cumbersome and sometimes even confusing to distinguish general CPO patterns, we suggest for all cases the convention

$$\lambda_1 \le \lambda_2 \le \lambda_3 \le \lambda_4; \quad \sum_{i=1}^{4} \lambda_i = 0.$$

We introduce a parametrization of $\lambda_i, i = 1, \ldots, 4$, by

$$\begin{aligned} \lambda_1 &= \lambda\,(-1 - 2S), \quad \lambda_3 = \lambda\,(1 - 2B), \\ \lambda_2 &= \lambda\,(-1 + 2S), \quad \lambda_4 = \lambda\,(1 + 2B), \end{aligned}$$

which characterizes any set of λ_i in terms of a degree of anisotropy (λ)

$$\lambda = -\frac{1}{2}(\lambda_1 + \lambda_2) = \frac{1}{2}(\lambda_3 + \lambda_4),$$

and the amounts to a bipolar (B), circular (C) and spherical (S) distribution

$$B = \frac{1}{2}\frac{\lambda_4 - \lambda_3}{\lambda_3 + \lambda_4}, \quad C = \frac{\lambda_3 - \lambda_2}{\lambda_3 + \lambda_4}, \quad S = \frac{1}{2}\frac{\lambda_2 - \lambda_1}{\lambda_3 + \lambda_4},$$

satisfying $B + C + S = 1; \quad 0 \le B, C, S \le 1; \quad 0 \le \lambda < \infty$.

Then the Bingham distribution [Eq. (15)] can be rewritten as

$$f_{\mathrm{B}}(x;\Lambda,A) = c_B^{-1}(\Lambda)\exp(\lambda_1)\exp\left(4\lambda\cos^2\frac{\omega_\tau}{2}\right)ds_3 \tag{16}$$

$$= c_B^{-1}(\Lambda)\exp(-\lambda_2)\exp(2\lambda\cos\omega_\tau)\,ds_3,$$

$$\cos^2\frac{\omega_\tau}{2} := B\cos^2\frac{\omega_b}{2} + \frac{C}{2}\cos^2\frac{\omega_c}{2} + S\cos^2\frac{\omega_s}{2}, \tag{17}$$

where ω_b, ω_c and ω_s are defined by Equation (9) as the orientation distances between x and the bipolar point $B(a_4)$, the circle $C(a_3, a_4)$, and the sphere $S(a_2, a_3, a_4) = a_1^{\perp}$, respectively. The distribution is constant for any fixed $\omega_\tau \in [0, \pi]$, which may be interpreted as an effective orientation distance between x and the support of the respective distribution.

In agreement with the classification by Prentice (1986), we distinguish bipolar ($B > S$), circular ($B = S$) and spherical ($B < S$) distributions (Fig. 1). The corresponding sets of modes are the bipolar point $B(a_4)$, the circle $C(a_3, a_4)$, and the sphere $S(a_2, a_3, a_4) = a_1^{\perp}$, respectively, where the respective distributions assume maximum value.

In case of either B, C or $S = 1$, i.e., the others $= 0$, the distribution depends only on one of the three distances (ω_b, ω_c or ω_s), referring to the rotationally

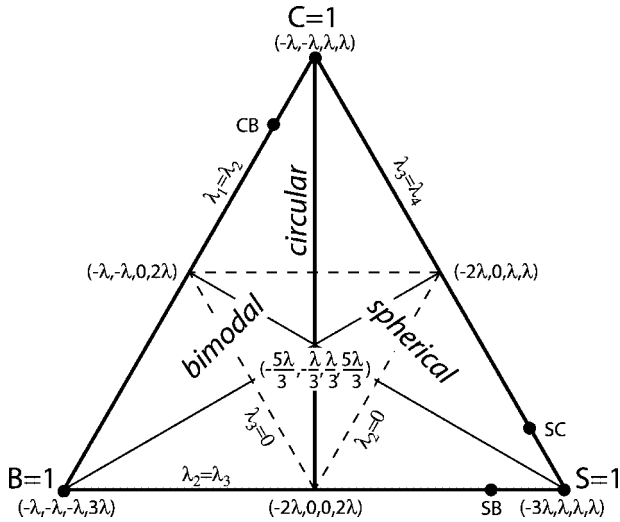

Figure 1. Parameter range of the Bingham distribution for constant λ represented as triangle with the rotationally invariant cases of a bipolar ($B = 1$), circular ($C = 1$) and spherical ($S = 1$) distribution at the corners.

Table 1. Parameters for the Rotationally Invariant Cases of the Bingham Distribution

Case	B	C	S	λ	λ_1	λ_2	λ_3	λ_4
Uniform	any	any	any	0	0	0	0	0
Bimodal	1	0	0	>0	$-\lambda$	$-\lambda$	$-\lambda$	3λ
Circular	0	1	0	>0	$-\lambda$	$-\lambda$	λ	λ
Spherical	0	0	1	>0	-3λ	λ	λ	λ

invariant bipolar, circular or spherical distribution, respectively (Table 1). If the Bingham distribution is rotationally invariant, it has minimum value in the orthogonal complement of the modal set with respect to $\mathbb{S}^3$, i.e., for the antimodes. It will be shown below that the rotationally invariant cases represent single component, fiber, and surface orientation distributions, respectively.

Normalization

By convention in texture analysis, the orientation probability density function and pole figures are normalized such that uniform distributions are equal to 1, i.e., $f_{\text{uniform}} \equiv 1$. With Equation (13) the normalization condition then reads

$$\int_{\mathbb{S}^3} f(x)\, ds_3(x) = 2\pi^2. \tag{18}$$

The normalization constant $c_B(\Lambda)$ for the Bingham distribution [Eq. (15)] is given by a hypergeometric function of matrix argument, ${}_1F_1(\frac{1}{2}; 2; \Lambda)$ (Bingham, 1964, 1974). Following a similar procedure as outlined by Wood (1988, 1993) and Eschner (1994) and using Equations (5) and (11), it reads

$$\begin{aligned}
c_B(\Lambda) &= \frac{1}{2\pi^2} \int_{\mathbb{S}^3} \exp\left\{ \sum_{i=1}^{4} \lambda_i (\mathrm{Sc}(a_i^* x))^2 \right\} ds_3(x) \\
&= \frac{1}{2\pi^2} \int_0^{\pi} dr \int_0^{\pi/2} \sin(2s)\, ds \int_0^{2\pi} dt \\
&\quad \exp[(\lambda_1 \cos^2 t + \lambda_2 \sin^2 t) \sin^2 s + (\lambda_3 \sin^2 r + \lambda_4 \cos^2 r) \cos^2 s] \\
&= \frac{1}{16\pi^2} \int_{-1}^{1} du \int_0^{2\pi} dr' \int_0^{4\pi} dt' \\
&\quad \times \exp[\lambda S(1-u) \cos t' + \lambda B(1+u) \cos r' + \lambda u] \\
&= \frac{1}{2} \int_{-1}^{1} du\; I_0(\lambda S(1-u)) I_0(\lambda B(1+u)) \exp(\lambda u),
\end{aligned}$$

with the substitutions $u = \cos(2s)$, $t' = 2t$, $r' = 2r$, the parameters $\lambda S = (\lambda_2 - \lambda_1)/4$, $\lambda B = (\lambda_4 - \lambda_3)/4$ and the modified Bessel functions

$$I_l(x) = \frac{1}{\pi} \int_0^{\pi} \exp(x \cos t) \cos(lt)\, dt; \tag{19}$$

it must be evaluated by numerical integration (Bingham, 1964; Onstott, 1980; Watson, 1983).

THE SPHERICAL RADON TRANSFORM

General Definition

The spherical Radon transform $\mathcal{R}$ associating a function $\mathcal{R}f : (\mathbb{S}^2 \times \mathbb{S}^2) \mapsto \mathbb{R}^1_+$ to an orientation probability density function $f : SO(3) \mapsto \mathbb{R}^1_+$ is defined as (Bunge, 1982; Cerejeiras, Schaeben, and Sommen, 2002; Helgason, 1959, 1999)

$$(\mathcal{R}f)(\mathbf{h}, \mathbf{r}) := \frac{1}{2\pi} \int_{G(\mathbf{h},\mathbf{r})} f(\boldsymbol{g})\, d\boldsymbol{g}, \tag{20}$$

where $G(\mathbf{h}, \mathbf{r}) := \{\boldsymbol{g} \in SO(3) \mid \boldsymbol{g}\,\mathbf{h} = \mathbf{r}\}$. In texture analysis it is known as "axis distribution function" (Bunge, 1982), also called "ideal" pole figure (Matthies, Vinel, and Helming, 1987).

The normal diffraction experiment as applied for texture measurements does not allow to distinguish a crystal direction $\mathbf{h}$ and its negative $-\mathbf{h}$. It is mathematically modeled by the (basic) *crystallographic* X-ray transform, which is provided by mean values of the Radon transform $(\mathcal{R}f)$ of an orientation probability density function f

$$(\mathcal{X}f)(\mathbf{h}, \mathbf{r}) = \frac{1}{2}((\mathcal{R}f)(\mathbf{h}, \mathbf{r}) + (\mathcal{R}f)(-\mathbf{h}, \mathbf{r})). \tag{21}$$

$(\mathcal{X}f)$ is usually referred to as bi-axial probability density function, also known as "reduced" pole figure. When $\mathbf{h}$ is considered rather as a parameter, $(\mathcal{X}f)$ is usually called $\mathbf{h}$-pole probability density function ("$\mathbf{h}$-pole figure"); when $\mathbf{r}$ is considered as a parameter, it is usually referred to as $\mathbf{r}$-inverse pole probability density function ("$\mathbf{r}$-inverse pole figure").

The spherical Radon transform of a uniform distribution is uniform; by convention it is $\mathcal{R}f_{\text{uniform}} \equiv 1$. It is normalized using Equations (12) and (14)

according to

$$\int_{\mathbb{S}^2} (\mathcal{R}f)(\mathbf{h}, \mathbf{r})\, ds_2(\mathbf{h}) = \int_{\mathbb{S}^2} (\mathcal{R}f)(\mathbf{h}, \mathbf{r})\, ds_2(\mathbf{r}) = 4\pi. \tag{22}$$

Integration Along Great Circles of $\mathbb{S}^3$

The spherical Radon transform [Eq. (20)] may be rewritten in quaternion notation as

$$(\mathcal{R}f)(\mathbf{h}, \mathbf{r}) = \frac{1}{2\pi} \int_{C(q_1, q_2)} f(q)\, dq = \frac{1}{2\pi} \int_0^{2\pi} f(q(t))\, dt, \tag{23}$$

where $q(t)$, $t \in [0, 2\pi)$, varies along the circle $C(q_1, q_2)$ of quaternions representing the set of rotations $G(\mathbf{h}, \mathbf{r})$ such that $q(t)\, \mathbf{h}\, q^*(t) = \mathbf{r}$ for all $q(t) \in C(q_1, q_2)$. This circle $C(q_1, q_2)$ can be generated by any two (noncolinear) of its constituents; for instance it is properly defined by a pair of orthonormal quaternions $q_1, q_2 \in \mathbb{S}^3$ as in Equation (8) by

$$C(q_1, q_2) = \{q(t) \in \mathbb{S}^3 | q(t) = q_1 \cos t + q_2 \sin t, t \in [0, 2\pi)\}. \tag{24}$$

It covers the integration path of Equation (20) twice, as it contains for each $q(t) \in C(q_1, q_2)$ also the negative quaternion $-q(t) = q((t + \pi) \bmod 2\pi)$, where both represent the same rotation. The quaternions $q_1, q_2 \in \mathbb{S}^3$ are given in terms of $\mathbf{h}, \mathbf{r} \in \mathbb{S}^2$ for $\mathbf{r} \neq \pm\mathbf{h}$ by

$$q_1 = \frac{1}{\|1 - \mathbf{rh}\|}(1 - \mathbf{rh}) = \cos\frac{\eta}{2} + \frac{\mathbf{h} \times \mathbf{r}}{\| \mathbf{h} \times \mathbf{r} \|} \sin\frac{\eta}{2}, \tag{25}$$

$$q_2 = \frac{1}{\|\mathbf{h} + \mathbf{r}\|}(\mathbf{h} + \mathbf{r}) = 0 + \frac{\mathbf{h} + \mathbf{r}}{\| \mathbf{h} + \mathbf{r}\|}, \tag{26}$$

with $\cos\eta = \mathbf{h} \cdot \mathbf{r}$ and

$$\|1 - \mathbf{rh}\| = \|\mathbf{h} + \mathbf{r}\| = \sqrt{2(1 + \mathbf{h} \cdot \mathbf{r})} = 2\cos\frac{\eta}{2}.$$

For $\mathbf{r} = \mathbf{h}$, the circle [Eq. (24)] with $q_1 = 1$ and $q_2 = \mathbf{h}$ represents rotations with angle $2t$ and axis $\mathbf{h}$. For $\mathbf{r} = -\mathbf{h}$, the circle [Eq. (24)] with $q_1 = \mathbf{v} \in \mathbb{S}^2, \mathbf{v} \cdot \mathbf{h} = 0$, and $q_2 = \mathbf{v} \times \mathbf{h}$ represents rotations with angle π and axis in the orthogonal complement $\mathbf{h}^\perp \cap \mathbb{S}^2$ of $\mathbf{h}$.

Radon Transform of the Bingham Distribution

The spherical Radon transform $\mathcal{R}$ of the Bingham distribution [Eq. (15)]

$$(\mathcal{R}[f_{\mathrm{B}}(\circ;\Lambda,A)])(\mathbf{h},\mathbf{r}) = \frac{1}{2\pi}\int_{\{x\in\mathbb{S}^3 \mid x\,\mathbf{h}\,x^*=\mathbf{r}\}} f_{\mathrm{B}}(x;\Lambda,A)\,ds_3(x)$$

follows after Equations (23) and (24) from integration along the circle $C(q_1, q_2)$ as

$$\begin{aligned}(\mathcal{R}f_{\mathrm{B}})(\mathbf{h},\mathbf{r}) &= c_B^{-1}(\Lambda)\frac{1}{2\pi}\int_0^{2\pi}\exp\left(\sum_{i=1}^{4}\lambda_i(\mathrm{Sc}(a_i^* q(t)))^2\right)dt\\ &= c_B^{-1}(\Lambda)\frac{1}{2\pi}\int_0^{2\pi}\exp(\xi+\upsilon\cos 2t+\zeta\sin 2t)\,dt\\ &= c_B^{-1}(\Lambda)\,\exp(\xi)I_0(\sqrt{\upsilon^2+\zeta^2}) \qquad (27)\end{aligned}$$

with the modified Bessel function $I_0(x)$ defined by Equation (19) and

$$\begin{aligned}\xi &= \frac{1}{2}\sum_{i=1}^{4}\lambda_i((\mathrm{Sc}(a_i^* q_1))^2+(\mathrm{Sc}(a_i^* q_2))^2),\\ \upsilon &= \frac{1}{2}\sum_{i=1}^{4}\lambda_i((\mathrm{Sc}(a_i^* q_1))^2-(\mathrm{Sc}(a_i^* q_2))^2),\\ \zeta &= \sum_{i=1}^{4}\lambda_i\,\mathrm{Sc}(a_i^* q_1)\,\mathrm{Sc}(a_i^* q_2).\end{aligned}$$

The quaternions q_1 and q_2 are given in terms of $\mathbf{h}$ and $\mathbf{r}$ by Equations (25) and (26). The numbers ξ and υ can be interpreted as the sum respectively difference of the effective (i.e., Λ-weighted) squared lengths of the quaternions q_1 and q_2, the number ζ as their effective (i.e., Λ-weighted) inner product. A formulation equivalent to Equation (27) was derived by Eschner (1994), where the numbers ξ, υ, ζ were expressed in terms of the parameters of the von Mises–Fisher matrix distribution, which is equivalent to the Bingham distribution (e.g., Prentice, 1986; Schaeben, 1996). It is emphasized that $(\mathcal{R}f_{\mathrm{B}})$ is not a Bingham distribution for $\mathbb{S}^2$ if one of its variables is considered as a mere parameter.

SPECIAL CASES

The Bingham distribution on $\mathbb{S}^3$ as introduced above can represent different types of CPO patterns, at least in case of triclinic crystal symmetry. In case of higher crystal symmetries, superpositions of Bingham distributions could be applied to represent crystallographic orientation distributions. More appropriate than superposition is the general approach by orientation probability density functions in the *crystallographic* exponential family as introduced by Boogaart (2002). With this restriction in mind, we shall use the terms crystallographic orientation and rotation synonymously.

In the following, we will discuss orientation distributions drawn from the rotationally invariant cases (Table 1) of the Bingham distribution f_{B} on $\mathbb{S}^3$. In particular, we shall analyze the corresponding pole figures. They express how a pattern of quaternions representing rotations given in terms of the parameters of the Bingham distribution transforms into the corresponding pattern of directions, which is provided by the spherical Radon transform ($\mathcal{R} f_{\mathrm{B}}$) defined on $\mathbb{S}^2 \times \mathbb{S}^2$.

Uniform Distribution

The family of Bingham distributions includes the uniform distribution for $\lambda = 0$. Obviously, as the orientation density function is constant, its spherical Radon transform is constant, too, and accomplishes the uniform distribution on $\mathbb{S}^2 \times \mathbb{S}^2$. Both densities are equal to 1 everywhere according to the normalization conventions [Eqs. (18) and (22)].

Bipolar Case: "Gaussian" Orientation Density Function

In the bipolar case of Table 1, the general Bingham distribution [Eq. (16)] with $\omega_\tau = \omega_b$ [Eq. (17)] degenerates to the rotationally invariant "bipolar" Watson distribution

$$f_{\mathrm{B}}(\omega_b; \lambda, a_4) = c_B^{-1}(\Lambda) \exp(-\lambda) \exp\left(4\lambda \cos^2 \frac{\omega_b}{2}\right) [ds_3(\omega_b)]. \qquad (28)$$

It depends only on $\omega_b = 2 \arccos(|\mathrm{Sc}(a_4^* x)|)$, which is the orientation distance between $B(a_4)$ and the random rotation x. If a_4 represents the identical rotation, i.e., $a_4 = 1$, then ω_b can be interpreted as the rotation angle of the random rotation x.

The set of modes $B(a_4) = \{\pm a_4\}$ is generated by a single quaternion and its negative representing the same rotation. The distribution is bipolar with maximum values at $\pm a_4$, and has minimum values in the orthogonal complement $a_4^\perp$ of a_4 with respect to $\mathbb{S}^3$, i.e., the sphere $S(a_1, a_2, a_3)$. For $\lambda \to \infty$, the δ–distribution with

support $\pm a_4$ is approached, i.e., an "Ideallage" of Grewen and Wassermann (1955).

With $\cos^2 \frac{\omega_b}{2} = (1 + \cos \omega_b)/2$, Equation (28) is rewritten as

$$f_b(\omega_b; S_b) = C_b^{-1}(S_b) \exp(S_b \cos \omega_b)[ds_3(\omega_b)],$$

which has been labeled "Gaussian" standard orientation density function in texture analysis (Matthies, 1980), where $S_b = 2\lambda$ and

$$C_b(S_b) = c_B(\Lambda) \exp(-\lambda) = I_0(S_b) - I_1(S_b)\,.$$

The spherical Radon transform follows from Equation (27) with $\xi = \lambda z_4$, $\sqrt{\upsilon^2 + \zeta^2} = \xi + \lambda$ and $z_4 = a_4 \mathbf{h}\, a_4^* \cdot \mathbf{r}$ to

$$(\mathcal{R} f_b)(\mathbf{h}, \mathbf{r}) = C_b^{-1}(2\lambda) \exp(\lambda\,(z_4 - 1)) I_0(\lambda(1 + z_4))$$

as given by Matthies (1980). It is only a function of the orientation distance $\omega_4 = \arccos z_4$ between a_4 and the circle $C(q_1, q_2)$ containing all q that transfer $\mathbf{h}$ into $\mathbf{r}$. The function is maximum for those pairs $(\mathbf{h}, \mathbf{r})$ for which $z_4 = 1$; it is minimum where $z_4 = -1$. For a fixed $\mathbf{h}_0 \in \mathbb{S}^2$, $(\mathcal{R} f_b)(\mathbf{h}_0, \mathbf{r})$ has its maximum in $\mathbf{r}_0 = a_4\, \mathbf{h}_0\, a_4^*$ and its minimum in $-\mathbf{r}_0$.

The basic crystallographic X-ray transform $(\mathcal{X} f_b)(\mathbf{h}_0, \mathbf{r})$ [Eq. (21)] is maximum in $\pm\mathbf{r}_0$ and minimum in the orthogonal complement $\mathbf{r}_0^\perp \cap \mathbb{S}^2$ of $\mathbf{r}_0$ with respect to $\mathbb{S}^2$, i.e. the great circle with pole $\mathbf{r}_0$.

Circular Case: "Gaussian" Fiber Orientation Density Function

In the circular case of Table 1, the general Bingham distribution [Eq. (16)] with $\omega_\tau = \omega_c$ [Eq. (17)] degenerates to the rotationally invariant "circular" distribution

$$\begin{aligned} f_{\mathrm{B}}(\omega_c; \lambda, a_3, a_4) &= c_B^{-1}(\Lambda) \exp(-\lambda) \exp\left(2\lambda \cos^2 \frac{\omega_c}{2}\right) ds_3(\omega_c) \\ &= c_B^{-1}(\Lambda) \exp(\lambda) \exp\left(-2\lambda \cos^2 \frac{\omega_c^\perp}{2}\right) ds_3(\omega_c) \end{aligned} \qquad (29)$$

with the set of modes $C(a_3, a_4)$ being the circle spanned by a_3 and a_4, where the distribution is maximum, and antimodes $C(a_1, a_2)$, where the distribution is minimum. The circle $C(a_3, a_4)$ represents the set of all rotations mapping $\mathbf{h}_c = a_4^* a_3$ on $\mathbf{r}_c = a_3 a_4^*$ [Eq. (10)]. The antimode circle $C(a_1, a_2)$ is the set of all rotations mapping $\mathbf{h}_c$ on $-\mathbf{r}_c$. For $\lambda \to \infty$, the δ-distribution with support $C(a_3, a_4)$ is approached, i.e., an "ideal fiber texture" of Grewen and Wassermann (1955).

The distribution depends only on the distances ω_c or $\omega_c^{\perp}$ of a random rotation x to $C(a_3, a_4)$ or $C(a_1, a_2)$, respectively, which sum up to π for any x, as shown by Equation (9) or equivalently by

$$\cos\omega_c = \mathbf{r}_c \cdot x\,\mathbf{h}_c\,x^* = -(-\mathbf{r}_c \cdot x\,\mathbf{h}_c\,x^*) = -\cos\omega_c^{\perp} = \cos(\pi - \omega_c^{\perp}).$$

The set $C_\tau(a_3, a_4) = \{x \in \mathbb{S}^3 \mid (\mathrm{Sc}(a_3^* x))^2 + (\mathrm{Sc}(a_4^* x))^2 = \tau^2\}$ can geometrically be interpreted as the set of unit quaternions in $\mathbb{S}^3$, which have constant modulus (length) when projected onto the two dimensional plane $E(a_3, a_4)$. Thus, the circular distribution [Eq. (29)] is rotationally invariant; it also is referred to as generalized Dimroth–Watson distribution (Watson, 1983).

In texture analysis, this case of the distribution has been labeled "Gaussian" standard fiber orientation density function (Matthies et al., 1988)

$$f_c(\omega_c;\lambda) = C_c^{-1}(\lambda)\,\exp(\lambda\cos\omega_c)[ds_3(\omega_c)]$$
$$C_c(\lambda) = c_B(\Lambda) = \sinh(\lambda)/\lambda$$

with dispersion parameter λ.

The spherical Radon transform (Matthies et al., 1988)

$$(\mathcal{R}f_c)(\mathbf{h},\mathbf{r}) = C_c^{-1}(\lambda)\,\exp(\lambda\,z_h\,z_r)I_0\big(\lambda\sqrt{1-z_h^2}\sqrt{1-z_r^2}\big)$$

is only a function of $z_h = \mathbf{h}\cdot\mathbf{h}_c$ and $z_r = \mathbf{r}\cdot\mathbf{r}_c$. It is maximum for those pairs $(\mathbf{h},\mathbf{r})$ for which $z_h z_r = 1$, i.e. for $\pm(\mathbf{h}_c,\mathbf{r}_c)$; it is minimum where $z_h z_r = -1$, i.e., for $\pm(\mathbf{h}_c,-\mathbf{r}_c)$.

For a fixed $\mathbf{h}_0 \in \mathbb{S}^2$, $(\mathcal{R}f_c)(\mathbf{h}_0,\mathbf{r})$ is rotationally invariant with respect to $\mathbf{r}_c$ and has its maximum in a small circle around $\mathbf{r}_c$ with aperture angle $\arccos(\mathbf{h}_0\cdot\mathbf{h}_c)$, which degenerates to a single maximum at $\pm\mathbf{r}_c$ for $\mathbf{h}_0\cdot\mathbf{h}_c = \pm 1$ or to a unique great circle with pole $\pm\mathbf{r}_c$ for $\mathbf{h}_0\cdot\mathbf{h}_c = 0$. $(\mathcal{R}f_c)(\mathbf{h}_0,\mathbf{r})$ is minimum at $-\mathbf{r}_c$ for $\mathbf{h}_0\cdot\mathbf{h}_c \geq 0$ (at $\mathbf{r}_c$ for $\mathbf{h}_0\cdot\mathbf{h}_c \leq 0$). Analogously, for a fixed $\mathbf{r}_0 \in \mathbb{S}^2$, $(\mathcal{R}f_c)(\mathbf{h},\mathbf{r}_0)$ is rotationally invariant with respect to $\mathbf{h}_c$ and has its maximum in a small circle around $\mathbf{h}_c$ with aperture angle $\arccos(\mathbf{r}_0\cdot\mathbf{r}_c)$.

For sufficiently large λ, the basic crystallographic X-ray transform $(\mathcal{X}f_c)(\mathbf{h}_0,\mathbf{r})$ [Eq. (21)] has its maximum value in two antipodally symmetric small circles centered at $\pm\mathbf{r}_c$ with aperture angle $\arccos(\mathbf{h}_0\cdot\mathbf{h}_c)$, which degenerate to two antipodally symmetric clusters at $\pm\mathbf{r}_c$ for $\mathbf{h}_0\cdot\mathbf{h}_c = \pm 1$ or to a unique great circle with pole $\pm\mathbf{r}_c$ for $\mathbf{h}_0\cdot\mathbf{h}_c = 0$. $(\mathcal{X}f_c)(\mathbf{h}_0,\mathbf{r})$ is minimum either on the great circle with pole $\pm\mathbf{r}_c$ (for small aperture angle) or in $\pm\mathbf{r}_c$ (for large aperture angle).

Spherical Case: "Gaussian" Surface Orientation Density Function

In the spherical case of Table 1, the general Bingham distribution [Eq. (16)] with $\omega_\tau = \omega_s$ [Eq. (17)] degenerates to the rotationally invariant "spherical" Watson distribution

$$f_{\mathrm{B}}(\omega_s; \lambda, a_1) = c_B^{-1}(\Lambda)\, \exp(-3\lambda)\, \exp\left(4\lambda\, \cos^2 \frac{\omega_s}{2}\right) ds_3(\omega_s) \tag{30}$$

$$= c_B^{-1}(\Lambda)\, \exp(\lambda)\, \exp\left(-4\lambda\, \cos^2 \frac{\omega_s^\perp}{2}\right) ds_3(\omega_s).$$

It depends only on $\omega_s = \pi - \omega_s^\perp$, where $\omega_s^\perp = 2 \arccos(|\mathrm{Sc}(a_1^* x)|)$ is the orientation distance between a_1 and the random rotation x. The distribution is multimodal with the set of modes $S(a_2, a_3, a_4)$, the sphere spanned by a_i, $i = 2, 3, 4$, and antimode $B(a_1) = \{\pm a_1\}$. If a_1 represents the identical rotation, i.e., $a_1 = 1$, then $\omega_s^\perp$ can be interpreted as the rotation angle of the random rotation x, and the set of modes consists of all pure quaternions representing rotations by angle π around any axis $\mathbf{q} \in \mathbb{S}^2$.

This distribution may be thought of as the "orthogonally complementary" or "inverse" distribution of the rotationally invariant bipolar distribution [Eq. (28)], as the sets of modes and antimodes interchange by switching the sign of λ. The actual density values of maxima and minima, however, do not relate in such a simple way between both distributions. For $\lambda \to \infty$, the δ-distribution with support $S(a_2, a_3, a_4)$ is approached, i.e., an "ideal $\widetilde{\omega} = \pi$ surface texture" (Matthies, Vinel, and Helming, 1987).

The set $S_\tau(a_2, a_3, a_4) = \{x \in \mathbb{S}^3 \,|\, (\mathrm{Sc}(a_2^* x))^2 + (\mathrm{Sc}(a_3^* x))^2 + (\mathrm{Sc}(a_4^* x))^2 = \tau^2\} \subset \mathbb{S}^3 \subset \mathbb{H}$ can geometrically be interpreted as the set of unit vectors in $\mathbb{S}^3$, which have constant modulus (length) when orthogonally projected onto the three dimensional hyperplane $F(a_2, a_3, a_4)$. Thus, the spherical distribution [Eq. (30)] is rotationally invariant.

In texture analysis, this case may be referred to as "Gaussian" standard surface orientation density function with dispersion $S_s = 2\lambda$

$$f_s(\omega_s; S_s) = C_s^{-1}(S_s)\, \exp(S_s\, \cos\, \omega_s)[ds_3(\omega_s)],$$

$$C_s(S_s) = c_B(\Lambda)\, \exp(\lambda) = I_0(S_s) + I_1(S_s).$$

The spherical Radon transform follows from Equation (27) with $\xi = -\lambda\, z_1$, $\sqrt{\upsilon^2 + \zeta^2} = \lambda - \xi$ and $z_1 = a_1\, \mathbf{h}\, a_1^* \cdot \mathbf{r}$ as

$$(\mathcal{R} f_s)(\mathbf{h}, \mathbf{r}) = C_s^{-1}(2\lambda)\, \exp(\lambda\,(1 - z_1)) I_0(\lambda(1 + z_1)).$$

It is only a function of the orientation distance $\omega_1 = \arccos z_1$ between a_1 and the circle $C(q_1, q_2)$ containing all q that transfer $\mathbf{h}$ into $\mathbf{r}$. The function is maximum for those pairs $(\mathbf{h}, \mathbf{r})$ for which $z_1 = -1$; it is minimum where $z_1 = 1$. For a fixed $\mathbf{h}_0 \in \mathbb{S}^2$, $(\mathcal{R}f_s)(\mathbf{h}_0, \mathbf{r})$ has its maximum in $\mathbf{r}_0 = -a_1\,\mathbf{h}_0\,a_1^*$ and its minimum in $-\mathbf{r}_0$.

The basic crystallographic X-ray transform $(\mathcal{X}f_s)(\mathbf{h}_0, \mathbf{r})$ [Eq. (21)] is maximum in $\pm\mathbf{r}_0$ and minimum in the orthogonal complement $\mathbf{r}_0^{\perp} \cap \mathbb{S}^2$ of $\mathbf{r}_0$ with respect to $\mathbb{S}^2$, i.e. the great circle with pole $\mathbf{r}_0$.

Examples

The family of Bingham distributions contains many more than just the perfect cases of rotationally invariant distributions. Variation of the parameters $\lambda_i, i = 1, \ldots, 4$, results in a wide diversity of patterns. The parameter range for constant anisotropy degree λ is mapped onto a triangle in Figure 1, where the corners correspond to the three rotationally invariant cases. General circular distributions map onto the central vertical line, which divides the parameter space between general bimodal distributions to the left from general spherical distributions to the right, in analogy to the classification given by Prentice (1986).

As examples, six different Bingham distributions are discussed in the following. They all have in common the modal quaternions $a_i, i = 1, \ldots, 4$, which are illustrated in Figure 2 by the vectors $\mathbf{r}_0 = a_i\,\mathbf{h}_0\,a_i^*$ in equal area projections, where $\mathbf{h}_0$ assumes four specific crystal directions, namely the three orthonormal basis vectors (100), (010), (001) plus an arbitrary pole (123). For simplicity a triclinic crystal is assumed with a unit cell spanned by crystallographic basis vectors that are mutually perpendicular and have length ratios of 4:6:9. The identity rotation is defined by (100) $\parallel RD$, (010) $\parallel TD$, (001) $\parallel ND$ = outward normal to projection. Projections of upper and lower hemisphere are distinguished by closed and open circles, respectively. The quaternion a_4 is chosen to correspond to the set of Euler angles $(\phi_1, \Phi, \phi_2) = (20^\circ, 50^\circ, 30^\circ)$. In order to form a set of four mutually

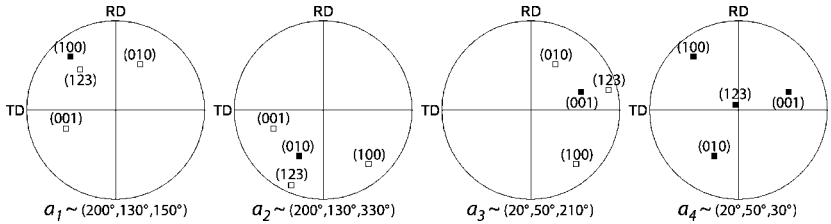

Figure 2. Four crystal orientations corresponding to the modes of an example distribution represented by equal area projections of specific crystallographic poles $\mathbf{h} = (hkl)$ on upper (closed symbols) and lower (open symbols) hemisphere.

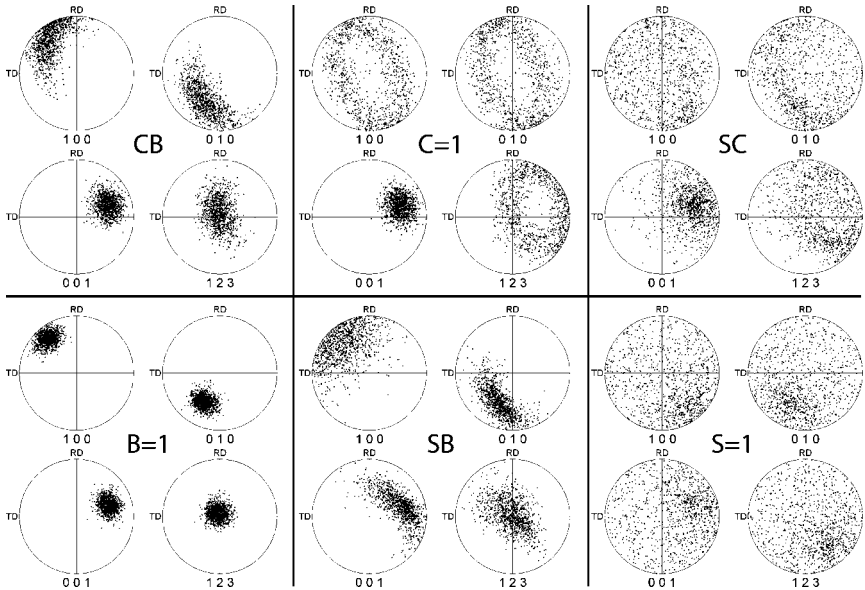

Figure 3. Radon transform (ideal pole figures) for populations of 1,000 orientations drawn from six selected Bingham distributions with parameters of Table 2, three rotationally invariant (B, C or $S = 1$) and three transitional cases (CB, SB, SC). For each case equal area projections are plotted for four crystallographic poles $\mathbf{h} = (hkl)$ on upper (closed symbols) and lower (open symbols) hemisphere.

orthogonal quaternions, the quaternions $a_i, i = 1, 2, 3$, must be derived from a_4 by rigid rotation by π about any three perpendicular directions, which are chosen here as the three basis vectors (100), (010), (001), i.e., $a_i = e_i a_4, i = 1, \ldots, 3$. Comparing a_1 and a_4, (100) is transformed into the same direction, but (010) and (001) are transformed into their respective opposite directions, and (123) points into completely different directions; the same holds analogously for a_2 and (010) as well as for a_3 and (001).

The spherical Radon transforms are plotted in Figure 3 for simulated populations of 1,000 crystal orientations derived from Bingham distributions for the three rotationally invariant cases and three intermittent cases representing transitions between pairs of the former three, all for a fixed value of $\lambda = 20$. The sets of shape parameters $(\lambda_1, \lambda_2, \lambda_3, \lambda_4)$ respectively $[B, C, S]$ are marked in Figure 1 and listed in Table 2.

Density estimates for the Radon transform ("ideal" pole figures, Fig. 4) and for the X-ray transform ("reduced" pole figures, inversion symmetry imposed, Fig. 5) are shown for the same cases, but a smaller anisotropy degree $\lambda \approx 5$ was used for the sake of better visualization. Characteristic features in Figures 3–5 will be discussed in the following.

Table 2. Parameters for the Six Example Cases of the Bingham Distribution

Case	B	C	S	λ	λ_1	λ_2	λ_3	λ_4
$B = 1$	1	0	0	20	−20	−20	−20	60
$C = 1$	0	1	0	20	−20	−20	20	20
$S = 1$	0	0	1	20	−60	20	20	20
CB	0.125	0.875	0	20	−20	−20	15	25
SC	0	0.125	0.875	20	−55	15	20	20
SB	0.125	0	0.875	20	−55	15	15	25

The *bipolar case* ($B = 1$) is represented by single rotationally invariant clusters around $\mathbf{r}_0 = a_4\,\mathbf{h}_0\,a_4^*$ in the $\mathbf{h}_0$-ideal pole figure and around $\pm\mathbf{r}_0$ in the $\mathbf{h}_0$-reduced pole figure for each $\mathbf{h}_0$. Because the X-ray transform is the mean of two related Radon transforms, maxima values in the reduced pole figures are about half as high as in the ideal ones.

The *transitional case CB* represents a partial fiber texture, i.e., it poses some but not complete freedom of rotation around (001). The maximum values are at the

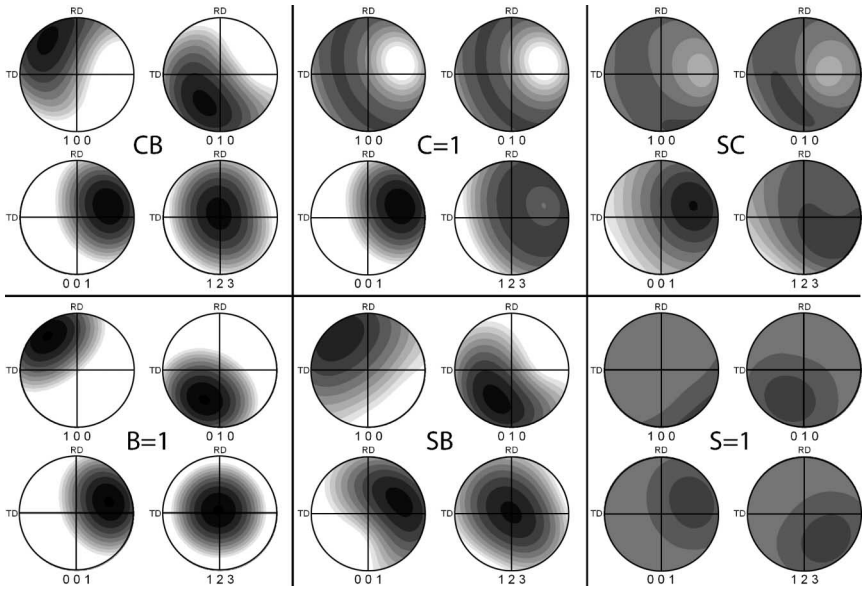

Figure 4. Radon transform (ideal pole figures) for six selected Bingham distributions; cases as in Figure 3 but with $\lambda = 5$. Contours represent domains of equal density using a logarithmic scale (0.03125, 0.0625, 0.125, 0.25, 0.5, 1.0, 2.0, 4.0, 8.0, 16.0 times uniform) on upper hemisphere in equal area projection.

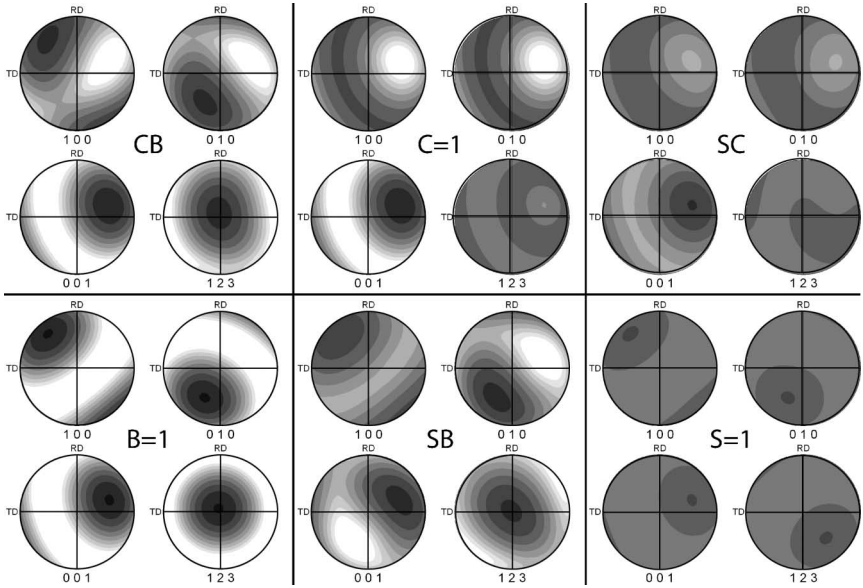

Figure 5. X-ray transform (reduced pole figures) for six selected Bingham distributions; cases and contours as in Figure 4.

same positions as in the bipolar case, but the shape of the surrounding distributions has changed. The (001)-pole figure remains rotationally invariant but with reduced density, while the maxima for (100) and (010) become elongated along the great circle with pole at the maximum of (001).

In the *circular case* ($C = 1$) representing a perfect fiber texture, this great circle is evenly occupied. The modes a_3 and a_4 correspond to the vectors $\mathbf{h}_c = (001)$ and $\mathbf{r}_c = a_4\,\mathbf{h}_c\,a_4^*$. All orientations along the circle $C(a_3, a_4)$ appear with equal frequency, i.e. for which (001) is fixed while the rotation around is arbitrary. All pole figures are rotationally invariant around the same direction $\mathbf{r}_c$. For $\mathbf{h}_0 = (100), (010)$ it is $\mathbf{h}_0 \cdot \mathbf{h}_c = 0$, so that ideal and reduced pole figures are identical, which does not hold in the general case like for $\mathbf{h}_0 = (123)$.

The *transitional case SB* allows partial freedom of rotation around (001) as well as around (010) and thus around any direction perpendicular to (100). In other words, it may be interpreted as reduced freedom in rotation around (100) compared to any other axes. This results in a widely scattered maximum for (100) and elongated maxima in the pole figures of (001) and (010), which do not follow any common great circle nor any other common path.

The *spherical case* ($S = 1$) shows comparably low maximum values at $\mathbf{r}_0 = -a_1\,\mathbf{h}_0\,a_1^*$, which are parallel to $a_4\,\mathbf{h}_0\,a_4^*$ for $\mathbf{h}_0 = (010), (001)$ but parallel to $-a_4\,\mathbf{h}_0\,a_4^*$ for $\mathbf{h}_0 = (100)$. Thus they are at the same directions like in the bipolar

case for (010) and (001) and at the opposite direction for (100). Apparently the former right handed system of maximum directions for (100), (010), (001) is converted to a left handed one. However, these maxima cannot be related to any single preferred orientation, because that handedness conversion is crystallographically not allowed. Instead, the maxima are explained by a preferred absence of orientations around a_1 and the density being widely distributed in the remainder, increasingly frequent with increasing distance from a_1. With imposed inversion symmetry, the reduced pole figures for (100), (010), (001) have their maximum values at exactly the same directions like in the bipolar case, though with much lower density and wider spread. However, any general pole figure, e.g., for (123), shows maximum values at completely different directions in the spherical compared to the bipolar case.

Finally, the *transitional case SC* illustrates the depletion of orientations around a_1 in the transition between the perfectly circular and spherical cases. The reduced pole figures for *SC* are hardly distinguishable from those for $C = 1$; they have very similar positions of maximum and minimum values but flatter density distributions.

CONCLUSIONS

- The Bingham distribution allows to represent a wide range of possible CPO patterns, including special cases which have already been used for classification and modeling in texture analysis. It will help to interpret experimental texture patterns, especially as they do normally not fit with any of those special cases but represent transitional distributions between the end members.
- There are other types of CPO patterns, which cannot be modeled by the Bingham distribution, in particular "cone fiber" textures (including the special case of "ring fiber" textures) as defined by Grewen and Wassermann (1955) and Matthies et al. (1988). They will be discussed in a subsequent contribution in terms of distributions in the crystallographic exponential family (Boogaart, 2002) of one order larger than the Bingham distribution.
- Quaternion algebra provides convenient tools to derive spherical Radon transforms from any particular Bingham distribution, i.e., pole figures for a variety of texture patterns. The examples in this study highlight some of the ambiguities, which arise when a texture pattern is attempted to be interpreted based only on a few particular pole figures.
- While this study was focused onto the analysis of crystallographic textures, similar procedures may be applied to the analysis of distributions of any kind of rotations or orientations. In Earth sciences such data sets may consist of correlated foliation/lineation pairs from field mapping, triaxial

palaeomagnetic data (Onstott, 1980), or palaeostress markers to be used in spherical geostatistics (Boogaart and Schaeben, 2002a,b).

DEDICATION AND ACKNOWLEDGMENTS

The authors would like to dedicate this contribution to Professor Heinrich Siemes, Aachen, on the occasion of his 75th birthday.

Heinrich Siemes was born on August 15, 1929. He is retired Professor of Mineralogy at the Department of Mining Engineering, Metallurgy, and Geosciences, Aachen University of Technology (Germany). For more than 30 years he has championed the development of computer applications in geosciences. He has developed and applied methods of fabric and texture analysis to study natural and experimental deformation processes of ores, and has practiced geostatistics in ore reserve estimation in South America. He has published numerous scientific papers contributing to applications of texture analysis; he is also coauthor (together with H. Akin) of the book "Praktische Geostatistik," Springer, Berlin, 1988.

We are indebted to Heinrich Siemes as our teacher and PhD supervisor (Schaeben, 1981; Kunze, 1991). He has continued to support us as part of his scientific family and helped us in many ways with stimulating advice and encouragements.

This study benefited largely from discussions during the workshops on "Textures in Geology" in Freiberg in 2000 and 2003, in particular with Gerald van den Boogaart and Kurt Helming. KK would like to acknowledge travel support for these occasions through Bergakademie Freiberg and DFG-Graduiertenkolleg "Räumliche Statistik".

REFERENCES

Altmann, S. L., 1986, Rotations, quaternions, and double groups: Oxford University Press, Oxford, 317 p.

Bingham, C., 1964, Distributions on the sphere and on the projective plane: Unpublished PhD Thesis, Yale University, 80 p.

Bingham, C., 1974, An antipodally symmetric distribution on the sphere: Ann. Statist., v. 2, no. 6, p. 1201–1225.

Boogaart, K. G. v. d., 2002, Statistics for individual crystallographic orientation measurements: Dissertation TU Freiberg, Shaker-Verlag, Aachen, 159 p.

Boogaart, K. G. v. d., and Schaeben, H., 2002a, Kriging of regionalized directions, axes, and orientations: I. Directions and axes: Math. Geol., v. 34, no. 5, p. 479–503.

Boogaart, K. G. v. d., and Schaeben, H., 2002b, Kriging of regionalized directions, axes, and orientations: II. Orientations: Math. Geol., v. 34, no. 6, p. 671–677.

Bunge, H. J., 1982, Texture analysis in materials science: Mathematical methods: Butterworths, London, p. 193.

Cerejeiras, P., Schaeben, H., and Sommen, F., 2002, The spherical X-ray transform: Math. Methods Appl. Sci., v. 25, no. 16–18, p. 1493–1507.

Eschner, T., 1994, Generalized model function for quantitative texture analysis, *in* Bunge, H. J., Siegesmund, S., Skrotzki, W., and Weber, K., eds., Textures of geological materials: DGM Informationsgesellschaft, Oberursel, p. 15–28.

Gürlebeck, K., and Sprößig, W., 1997, Quaternionic and Clifford calculus for physicists and engineers: Wiley, Chichester, 371 p.

Grewen, J., and Wassermann, G., 1955, Über die idealen Orientierungen einer Walztextur: Acta Metall., v. 3, no. 4, p. 354–360.

Helgason, S., 1959, Differential operators on homogeneous spaces: Acta Math., v. 102, no. 3–4, p. 239–299.

Helgason, S., 1999, The Radon transform: Birkhäuser, Boston, 188 p.

Kuipers, J. B., 1999, Quaternions and rotation sequences: A primer with applications to orbits, aerospace, and virtual reality: Princeton University Press, Princeton, 371 p.

Kunze, K., 1991, Zur quantitativen Texturanalyse von Gesteinen: Bestimmung, Interpretation und Simulation von Quarzteilgefügen: Dissertation RWTH Aachen, Veröff. Zentralinstitut Physik der Erde Nr. 117, Potsdam, 136 p.

Matthies, S., 1980, Standard functions in the texture analysis: Phys. Status Solidi B, v. 101, no. 2, p. K111–K115.

Matthies, S., Vinel, G. W., and Helming, K., 1987, Standard distributions in texture analysis, vol. I: Akademie Verlag, Berlin, 442 p.

Matthies, S., Helming, K., Steinkopff, T., and Kunze, K., 1988, Standard distributions for the case of fibre textures: Phys. Status Solidi B, v. 150, no. 1, p. K1–K5.

Meister, L., and Schaeben, H., 2004, A concise quaternion geometry of rotations: Math. Methods Appl. Sci. (in press).

Onstott, T. C., 1980, Application of the Bingham distribution function to paleomagnetic studies: J. Geophys. Res., v. 85, no. B3, p. 1500–1510.

Prentice, M. J., 1980, Orientation statistics without parametric assumptions: J. R. Stat. Soc., v. B48, no. 2, p. 214–222.

Schaeben, H., 1981, Mathematische Methoden der Analyse von Richtungsgefügen: Unpublished Dissertation, RWTH Aachen, 252 p.

Schaeben, H., 1996, Texture approximation or texture modelling with components represented by the von Mises–Fisher matrix distribution on $SO(3)$ and the Bingham distribution on S^4_+: J. Appl. Cryst., v. 29, no. 5, p. 516–525.

Watson, G. S., 1983, Statistics on spheres: Wiley, New York, 238 p.

Wenk, H.-R. (ed.), 1985, Preferred orientation in deformed metals and rocks: An introduction to modern texture analysis: Academic Press, Orlando, 610 p.

Wood, A. T. A., 1988, Some notes on the Fisher–Bingham family on the sphere: Comm. Stat. Theory Methods, v. 17, no. 11, p. 3881–3897.

Wood, A. T. A., 1993, Estimation of the concentration parameters of the Fisher matrix distribution on $SO(3)$ and the Bingham distribution on $\mathbb{S}_q$, $q \geq 2$: Austral. J. Statist., v. 35, no. 1, p. 69–79.

APPENDIX: REAL QUATERNIONS

The algebra of real quaternions $\mathbb{H}$ is the tuple of $\mathbb{R}^4$ endowed with the operation of quaternion multiplication; furtheron, $\mathbb{H}$ is referred to as skew-field of real quaternions. Its exposition follows Altmann (1986), Gürlebeck and Sprößig (1997) as well as Kuipers (1999).

Skew-Field of Real Quaternions

An arbitrary quaternion $q \in \mathbb{H}$ is composed of a scalar part Scq and a vector part Vec$q$

$$q = q_0 + \mathbf{q} = \mathrm{Sc}q + \mathrm{Vec}q$$

with $q_0 = \mathrm{Sc}q$ and $\mathbf{q} = \sum_{i=1}^{3} q^i e_i = \mathrm{Vec}q$. The basic elements $e_i, i = 1, 2, 3$, fulfil the relations

$$\begin{aligned} &\text{(i) } e_i^2 = -1, \quad i = 1, 2, 3; \\ &\text{(ii) } e_1 e_2 = e_3, \quad e_2 e_3 = e_1, \quad e_3 e_1 = e_2; \\ &\text{(iii) } e_i e_j + e_j e_i = 0, \quad i, j = 1, 2, 3; \quad i \neq j. \end{aligned} \tag{31}$$

If $q = \mathbf{q}$, i.e., Sc$q = 0$, then q is called a pure quaternion. The subset of all pure quaternions is denoted Vec$\mathbb{H}$. The subset of all scalars may be denoted Sc$\mathbb{H}$. In this way $\mathbb{R}$ and $\mathbb{R}^3$ are embedded in $\mathbb{H}$. For $q \in \mathrm{Vec}\mathbb{H}$, q and $\mathbf{q}$ are identified, i.e., $q = \mathbf{q}$.

The product of two quaternions $p,\ q \in \mathbb{H}$ follows from Equation (31) as

$$\begin{aligned} pq &= p_0 q_0 - \mathbf{p} \cdot \mathbf{q} + p_0 \mathbf{q} + q_0 \mathbf{p} + \mathbf{p} \times \mathbf{q}, \\ \mathrm{Sc}(pq) &= p_0 q_0 - \mathbf{p} \cdot \mathbf{q}, \mathrm{Vec}(pq) = p_0 \mathbf{q} + q_0 \mathbf{p} + \mathbf{p} \times \mathbf{q}, \end{aligned}$$

where $\mathbf{p} \cdot \mathbf{q}$ and $\mathbf{p} \times \mathbf{q}$ are the standard inner and wedge products in $\mathbb{R}^3$, respectively.

Conjugation

The quaternion $q^* = \mathrm{Sc}q - \mathrm{Vec}q$ is called the conjugate of q. With conjugated quaternions it is possible to represent the scalar and vector part in an algebraic fashion as

$$\begin{aligned} q_0 = \mathrm{Sc}q &= \tfrac{1}{2}(q + q^*) \\ \mathbf{q} = \mathrm{Vec}q &= \tfrac{1}{2}(q - q^*) \end{aligned} \tag{32}$$

It holds that $(pq)^* = q^* p^*$. Since $\mathrm{Vec}q^* = -\mathrm{Vec}q$, conjugation of pure quaternions means change of sign, i.e., $\mathbf{q}^* = -\mathbf{q}$.

Norm and Spherical Distance

The norm $\|q\|$ of a quaternion q as defined by

$$qq^* = q^*q = q_0^2 + (q^1)^2 + (q^2)^2 + (q^3)^2 =: \|q\|^2$$

coincides with the Euclidean norm of q regarded as an element of the vector space $\mathbb{R}^4$. A quaternion q with $\|q\| = 1$ is called a unit quaternion. Further it is $\|pq\| = \|p\|\,\|q\|$.

The usual Euclidean inner product in the space $\mathbb{R}^4$ corresponds to the scalar part of pq^*, i.e., considering quaternions as vectors in $\mathbb{R}^4$ it is

$$p \cdot q = p_0q_0 + p^1q^1 + p^2q^2 + p^3q^3 = \mathrm{Sc}(pq^*).$$

Let $\mathbb{S}^2$ denote the unit sphere in $\mathrm{Vec}\,\mathbb{H} \simeq \mathbb{R}^3$ of all unit vectors, and $\mathbb{S}^3$ the sphere in $\mathbb{H} \simeq \mathbb{R}^4$ of all unit quaternions. In complete analogy to the unit sphere in $\mathbb{R}^4$, $\mathrm{Sc}(pq^*)$ provides a canonical measure for the spherical distance of unit quaternions $p, q \in \mathbb{S}^3$, which is given by the angle $\omega_{pq} = 2\arccos(\mathrm{Sc}(pq^*))$ between two rotations represented by p and q, also called 'orientation distance' in texture analysis.

Inversion

Each non-zero quaternion q has a unique inverse $q^{-1} = q^*/\|q\|^2$ with $\|q^{-1}\| = \|q\|^{-1}$. For unit quaternions it is $q^{-1} = q^*$; for pure unit quaternions it is $\mathbf{q}^{-1} = -\mathbf{q}$, thus $\mathbf{qq} = -1$.

Orthogonality

Two quaternions $p, q \in \mathbb{H}$ are said to be orthogonal, if pq^* is a pure quaternion, i.e., $pq^* \in \mathrm{Vec}\mathbb{H}$, or according to Equation (32)

$$2\,\mathrm{Sc}(pq^*) = pq^* + qp^* = 0.$$

Two unit quaternions $p, q \in \mathbb{S}^3$ are orthogonal, if and only if $p = \mathbf{v}q \in \mathbb{S}^2q$ for some pure unit quaternion $\mathbf{v} \in \mathbb{S}^2$; they are called orthonormal quaternions.

Orthogonality of two quaternions does not imply orthogonality of their vector parts and vice versa, unless they are pure quaternions.

Representation by Rotation Axis and Angle

An arbitrary quaternion permits the representation

$$q = \|q\|\left(\frac{q_0}{\|q\|} + \frac{\mathbf{q}}{\|\mathbf{q}\|}\frac{\|\mathbf{q}\|}{\|q\|}\right) = \|q\|\left(\cos\frac{\omega}{2} + \mathbf{n}\,\sin\frac{\omega}{2}\right)$$

with $\omega = 2\arccos(q_0/\|q\|)$, $\mathbf{n} = \mathbf{q}/\|\mathbf{q}\|$, and $\|\mathbf{q}\|^2 = \mathbf{q}\mathbf{q}^*$ considering $\mathbf{q}$ as a pure quaternion. For unit quaternions the representation

$$q = q_0 + \mathbf{q} = \cos\frac{\omega}{2} + \mathbf{n}\,\sin\frac{\omega}{2} \tag{33}$$

is often applied in the context of rotations, where $\mathbf{n} = \mathbf{q}/\|\mathbf{q}\| \in \mathbb{S}^2$ denotes the axis and $\omega = 2\arccos(q_0) \in [0, \pi]$ the angle of a right-handed (positive) rotation about $\mathbf{n}$.